Characterizing a model food gel containing bubbles and solid inclusions using ultrasound

Anatoliy Strybulevych,[ab] Valentin Leroy,[a] M. G. Scanlon[b] and J. H. Page*[a]

Received 10th May 2007, Accepted 10th August 2007
First published as an Advance Article on the web 7th September 2007
DOI: 10.1039/b706886g

Ultrasonic spectroscopy is used to characterize a model aerated food system consisting of agar gel in which both bubbles and polystyrene beads are embedded. By exploiting the distinct frequency dependence of each inclusion's acoustic resonances, it is demonstrated that the sizes of the bubbles and beads can be measured by ultrasound even when the size distributions are so similar that these inclusions are difficult to distinguish in optical images. While these results demonstrate the potential for applying ultrasonic spectroscopy to evaluate any soft heterogeneous material in which both bubbles and solid inclusions are present, the technique is especially relevant for functional foods, in which solid functional ingredients must be incorporated without degrading the aerated structure of the food and causing unacceptable quality impairment.

Introduction

Most processed foods are complex, multi-structured, heterogeneous, soft materials,[1,2] and the quality of these foods is strongly dependent on correctly manipulating their structure during processing.[3,4] The nutritional quality of food materials is also affected by the structural organization of molecules,[5] with (in some instances) markedly different bioavailability depending on the physico-chemical environment in which the molecules are situated.[6] In recent years, concerns about diet-related disease have driven the growth of a functional foods industry.[2,7] Since functional foods produce physiological health-promoting effects that cannot be gleaned from a proximate analysis of their macro- and micro-nutrients,[7,8] then microstructure manipulation during processing is key to the successful formulation of effective functional foods.

One means of creating functional foods is to bolster the nutritional efficacy of a conventional food by adding specific components.[7–9] However, adding these components can impair the original quality of the food, an outcome particularly evident in aerated foods such as bread, cakes, ice cream and other processed desserts.[10–13] For instance, in breadmaking, adding components such as bran can physically disrupt the thin film that surrounds growing gas bubbles in the dough, thus limiting retention of the carbon dioxide that is critical to good structure and volume in the loaf.[10] Given the weak mechanical properties of foams[14,15] and other aerated systems,[16] coupled with their propensity for dynamic changes in structure,[15–18] any interactions between added components and the original aerated structure are expected to disrupt the final structure, and hence reduce consumer acceptability, of these soft materials.

[a]*Department of Physics and Astronomy, University of Manitoba, Winnipeg, MB, Canada R3T 2N2. E-mail: jhpage@cc.umanitoba.ca; Fax: +1 204 474 7622; Tel: +1 204 474 9852*
[b]*Department of Food Science, University of Manitoba, Winnipeg, MB, Canada R3T 2N2. Fax: +1 204 474 7630; Tel: +1 204 474 6480*

To preserve better the original quality while maximizing the nutritional benefits, it is necessary to control interactions between added components and the dynamically-evolving distributions of bubbles during the various food process operations[19] that will create the functional food. Therefore, techniques are needed that will simultaneously determine the concentration and sizes of both bubbles and inclusions and preferably monitor interactions between them in real time. Given the opacity of most food materials, techniques that are non-destructive and applicable to optically opaque materials are especially desirable. A technique with the potential to address most of these desiderata is ultrasonic spectroscopy.

Ultrasonic spectroscopy is a technique in which low-intensity ultrasonic pulses are propagated into a material, and their frequency dependence is used to interrogate the material's mechanical behaviour.[20–22] The phase velocity and attenuation coefficient can be measured as a function of frequency using Fourier analysis to provide information on the mechanical properties and structure of the material through which the pulse has travelled (*e.g.* see ref. 23). Both the phase velocity and the attenuation coefficient can be markedly affected by structural heterogeneities where a difference in the acoustic impedance exists. For example, the large density and velocity difference between gases and condensed matter dictates a large acoustic impedance mismatch, leading to dramatic resonance effects that substantially modify the propagation of sound over a range of frequencies.[24] Therefore, ultrasonic spectroscopy appears suitable for investigations of the disruption of the aerated structure of soft materials to which nutrient inclusions are added.

The aim of this paper is to show that ultrasonic spectroscopy can resolve different types of inclusions in soft materials—specifically bubbles and relatively "hard" inclusions of comparable size. In this way, we show for a model aerated food system that ultrasonic spectroscopy is a promising technology for the functional foods industry because of its potential to identify interactions between "nutrient inclusions" and bubbles.

Materials and methods

Experiments were performed on three systems made from a matrix material of agar gel containing (1) bubbles, (2) polystyrene (PS) beads, and (3) bubbles and PS beads together, so that the underlying physics relating mean size, concentration and size distribution to ultrasonic data could be critically examined. Agar is a transparent gel, allowing independent measurements of the sizes and concentrations of the inclusions to be made by optical imaging techniques. Agar gel's acoustic properties are very close to those of water and do not show any unusual features as a function of frequency.

Agar gels of 2% concentration were prepared by dissolving granulated agar in distilled water and heating. The PS beads had a mean diameter of 250 μm (size range 149–350 μm) and were purchased from Bangs Laboratories, Inc. (Fishers, IN, USA). The PS beads were added to the gel at about 60 °C. Bubbles were entrained in the gel (or gel with PS beads) when the liquid sol was injected into the sample cell at high speed with a syringe, and the bubbles were then entrapped as the sol gelled. The samples were stirred continuously with a magnetic stirrer in order to obtain uniform distributions of the beads and/or bubbles in the gel until the gel temperature was lowered below approximately 55 °C and the gel was sufficiently viscous to trap the inclusions in place. After gelling of the agar dispersion, 15-mm-thick slabs were cut with a trimming blade. Pictures of both surfaces were taken before and after the experiments in order to measure the concentration and size distribution of the inclusions. The bubble and PS beads size distributions were determined from the pictures using the ImageJ software package (http://rsb.info.nih.gov/ij/, National Institutes of Health, Bethesda, MD, USA).

The ultrasonic experiments were carried out in a water tank at room temperature, by placing the samples in the path between a generating and a detecting transducer. Transducers with central frequencies of 40, 100, 250, 500 kHz, 1, 2.25 or 5 MHz were used. An arbitrary waveform generator (Agilent 33220A) and broadband power amplifier (Amplifier Research Model 250L) were used to generate and amplify the input signal that was applied to the generating transducer. Reference (water-path-only) and through-sample signals were detected by either a second transducer or a hydrophone, amplified and recorded on a digital oscilloscope (Tektronix TDS544A). The reference signal was measured so that the incident waveform could be determined, the latter being obtained from the reference pulse by shifting its arrival time by the time taken to travel in water through a distance equal to the sample thickness.

The attenuation coefficient, α, and phase velocity, v, were determined by comparing the magnitudes and phases of the fast Fourier transforms of the transmitted sample signal relative to the incident wave pulse:

$$\alpha = -2[\mathrm{In}(A_S/A_I)]/L \tag{1}$$

$$v = \omega L/(\phi_S - \phi_I) \tag{2}$$

Here ω, A, ϕ and L are the angular frequency, Fourier magnitude, cumulative phase and the sample thickness, respectively, and the subscripts S and I represent the through-sample and incident waveforms, respectively. Since the acoustic impedance of the sample differs from that of the surrounding medium, it was also necessary to correct for the reduction in the magnitude and possible phase shift of the transmitted pulse when crossing the sample interfaces.[24]

Results and discussion

(a) Gel with bubbles

It is known that the presence of bubbles in a liquid dramatically modifies the propagation of sound.[25,26] In particular, the velocity and attenuation as a function of frequency exhibit peaks whose shape and position are related to the radius distribution of the bubbles. Sound propagation in bubbly media of uniformly sized bubbles with radius R_0 can be described in terms of the frequency dependence of the complex wave vector k as

$$k^2 = k_M^2 + 4\pi N \frac{R_0\,\omega^2}{\omega_0^2 - \omega^2 - i\omega\Gamma} \tag{3}$$

where $k_M = \omega/v_M$ and v_M are the wave vector and velocity in the matrix, N is the number of bubbles per unit volume, and Γ is the damping factor, which includes radiating, viscous and thermal loss mechanisms. The resonance frequency ω_0 is known as the Minnaert angular frequency and is given by

$$\omega_0 \approx \frac{1}{R_0}\sqrt{\frac{3\gamma P_0}{\rho}} \tag{4}$$

where γ is the ratio of the heat capacities of the gas in the bubble, P_0 is the static pressure of the gas, and ρ the mass density of the matrix.

In the case of viscoelastic media, the complex frequency-dependent shear modulus shifts the Minnaert frequency to a higher value and leads to additional attenuation. By accounting for this effect, a good approximation for ω_0 is[27]

$$\omega_0 \approx \frac{1}{R_0}\sqrt{\frac{3\gamma P_0 + 4\mu'}{\rho}} \tag{5}$$

where μ' is the real part of the matrix shear modulus.

Eqn (3) is written for the case when all the bubbles are the same size. Its extension to the case when there is a distribution of different bubble sizes is

$$\begin{aligned} k^2 &= k_M^2 + 4\pi \int N(R) f(R,\omega)\,\mathrm{d}R \\ &= k_M^2 + 4\pi \int N(R) \frac{R\omega^2\,\mathrm{d}R}{\omega_0^2 - \omega^2 - i\omega\Gamma}, \end{aligned} \tag{6}$$

where $N(R)\mathrm{d}R$ is the number of bubbles with radius between R and $R + \mathrm{d}R$ per unit volume, and $f(R,\omega)$, given by the second term on the right hand side of eqn (3), is the scattering function of a bubble with radius R at frequency $\omega/2\pi$. The phase velocity and the attenuation are then determined from eqn (6) as

$$v = \omega/\Re e(k) \tag{7}$$

$$\alpha = 2\Im m(k) \tag{8}$$

The frequency dependence of the phase velocity and attenuation near resonance not only depends on the concentration and the size distribution of the bubbles incorporated in the medium, but is also affected by the physical properties of the gas fraction and matrix. The most relevant parameters are the volume fraction of bubbles, Φ, the gas pressure P_0, the parameters characterizing the bubble size distribution, as well as the density, phase velocity, and the real and imaginary parts of the shear modulus of the matrix. The influence of these parameters on the acoustic properties of bubbly media has been discussed in detail by Leroy *et al.*[24]

A typical picture of the bubbly sample and a histogram of measured radii are presented in Fig. 1a and 1b. It was found that the bubble sizes are well represented by a log-normal distribution

$$N(R) = \frac{N_{\text{tot}}}{\sqrt{2\pi}\sigma_{\text{LN}}R}\exp\left[-\frac{(\ln(R/R_0))^2}{2\sigma_{\text{LN}}^2}\right], \qquad (9)$$

where N_{tot} is the total number of bubbles per unit volume, R_0 = 0.115 mm is the median radius, and σ_{LN} = 0.23 is the logarithmic standard deviation. The total volume fraction, Φ, was also determined from the pictures by measuring the number of bubbles and their radii within the volume V_{picture}, defined by the known dimensions of the frame and depth of focus in the image:

$$\Phi = \frac{\sum_n \frac{4}{3}\pi R_n^3}{V_{\text{picture}}}, \qquad (10)$$

For the particular case shown in Fig. 1, Φ is equal to 0.75%.

All the model parameters except for the shear modulus were thus determined from our measurements. In the literature,[28] the shear modulus for a 2% agar gel is given as $\mu' \approx 55$ kPa and $\mu'' \approx 2.5$ kPa for frequencies up to 400 Hz. We also performed an experiment on a single 400-μm-radius bubble trapped in agar gel, and measured a Minnaert frequency of 10 kHz, which is consistent with a value of $\mu' \approx 55$ kPa [eqn (5)] at this frequency. Thus, the shear modulus appears to be independent of frequency in this range, enabling us to use this value for theoretical calculations. Fig. 1 shows a comparison of the experimental values of attenuation and phase velocity with theoretical predictions of the model [eqn (6)], as calculated from the real and imaginary parts of the wave vector. Note that there are no adjustable parameters in this theoretical calculation. The agreement between theory and experiment is very good for attenuation over the entire frequency range studied, with the theory reproducing the large and wide peak in attenuation that is observed near and above the Minnaert frequency. The theory also predicts the trends of phase velocity at high frequencies quite well, although the correspondence between experiment and theory deteriorates below 0.2 MHz, where the velocity is so large that the phase shift is very small and difficult to measure accurately. We want to stress that the resonance occurs when the wavelength is much bigger than R_0 ($\lambda_{\text{M}} = v_{\text{M}}/f$ = 15 mm at 100 kHz for v_{M} = 1.5 km s^{-1} (see Table 1), while the measured median radius of the bubbles is about 0.1 mm). Thus, the effective medium approach implicit in the theoretical model, which is applicable to the long wavelength regime ($\lambda_{\text{M}} \gg R$), is expected to be valid for describing the acoustic resonances of bubbles in

Table 1 Density, longitudinal velocity v_{l}, shear velocity v_{s} and attenuation for 2% agar gel and PS beads. The density of agar was determined by weighing a sample of known volume, and the PS density was measured by creating a neutrally buoyant suspension in a mixture of light and heavy water. For agar, the longitudinal velocity was measured in a separate experiment on pure gel, while the shear velocity is calculated from data in ref. 28. The attenuation in agar was similar to water and is negligible for these calculations. The values of longitudinal velocity and attenuation in the PS beads are taken from the literature,[33,34] while the corresponding velocity for shear waves was found from the best fit of the model to the experimental data

	ρ/g cm^{-3}	v_{l}/mm μs^{-1}	v_{s}/mm μs^{-1}	α_{l}/mm^{-1} MHz^{-1}	α_{s}/mm^{-1} MHz^{-1}
Agar	1.01	1.495	0.007	—	—
PS beads	1.044	2.35	1.02	0.0066	0.015

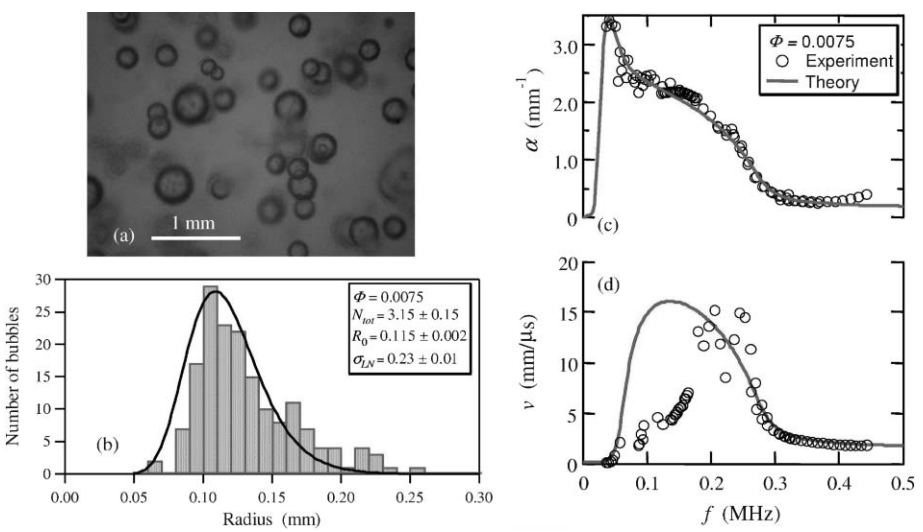

Fig. 1 (a) Sample image; (b) histogram of the bubble size distribution; and frequency dependence of (c) attenuation and (d) phase velocity for bubbles in a 2% agar gel.

gels, as well as in water. Furthermore, the good agreement between experiment and theory indicates that eqn (5) gives an accurate way of extending the acoustic resonance model for bubbly liquids to viscoelastic media, such as gels, that possess a shear modulus.

It is also worth emphasizing that the distinct character of the bubble resonance in a gel is similar to that in water. The maximum attenuation near resonance occurs at the Minnaert frequency ω_0 for a bubble of a given size, but the attenuation remains large for a range of frequencies above ω_0 up to the frequency ω_1 where the wavelength becomes comparable to the average spacing between the bubbles. Thus the attenuation peak becomes wider as the bubble concentration increases, because for the frequency range $\omega_0 < \omega < \omega_1$ the bubbles respond in phase opposition to the incident wave, and, as a result, k^2 in eqn (6) becomes negative, giving rise to a regime of large attenuation. The phase velocity is very small at low frequencies because the low frequency response is dominated by the large compressibility of the bubbles,[29] but rises sharply near the Minnaert frequency, reaching its peak value at a frequency above ω_0. At its peak, the velocity is much larger than the velocity of the pure gel, the value that is approached at high frequencies. Thus, one of the remarkable characteristics of bubble resonances is the very large range of phase velocity values that is encountered—a variation of more than two orders of magnitude for the case considered in Fig. 1.

(b) Gel containing only PS beads (model solid nutrient inclusions)

Solid inclusions have very different acoustic signatures to bubbles, as shown by the data in Fig. 2 for agar gel containing a 2% concentration of PS beads. This figure displays a typical image of part of the sample, a histogram of the particle size distribution, and the frequency dependence of the attenuation and phase velocity. From Fig. 2b, it can be seen that the particle size distribution of PS beads is very similar to the bubble size distribution shown in Fig. 1b. However, the lowest frequency resonance of the polystyrene bead system is observed at much higher frequencies. Also the magnitude of the changes in both attenuation and velocity are much less for the solid particles than for the bubbles, even though the PS concentration is more than two times greater.

To interpret the velocity and attenuation data, we need a model that describes the acoustic properties of a randomly positioned dispersion of solid PS beads embedded in a homogenous matrix. At high frequencies, where $\lambda \ll R$, the propagation of the sound wave is determined by the individual properties of each component, depending on which region the wave is in. At low frequencies, where $\lambda \gg R$, the wavelength is too large to resolve the individual scatterings, and wave propagation is determined by an average of the properties of the PS beads and matrix. This behaviour is well described by the coherent potential approximation (CPA).[30] However, the interesting behaviour seen in Fig. 2 occurs in the intermediate-frequency regime where $\lambda \sim R$; then, the wave is able to resolve the scatterers and the CPA approximation breaks down, requiring a different approach. In this intermediate frequency regime, the behaviour of wave transport in the gel containing polystyrene beads can be described by an effective medium model based on the spectral function approach (SpFA),[23,31,32] which allows the ultrasonic spectra to be related to bead size and concentration.

To describe the essential ideas of the spectral function approach, we illustrate the method for scalar waves, thereby avoiding writing down the additional mathematical complexity in the equations needed to account for the density difference and shear velocity of the PS beads. (These effects are nonetheless taken into account in the full calculations, whose results are shown below.) Since the gel shear velocity is very small (more than two orders of magnitude less than the longitudinal velocity, Table 1), its effect on the propagation of longitudinal waves in the effective medium can be neglected, so that the SpFA model developed for liquid suspensions can be

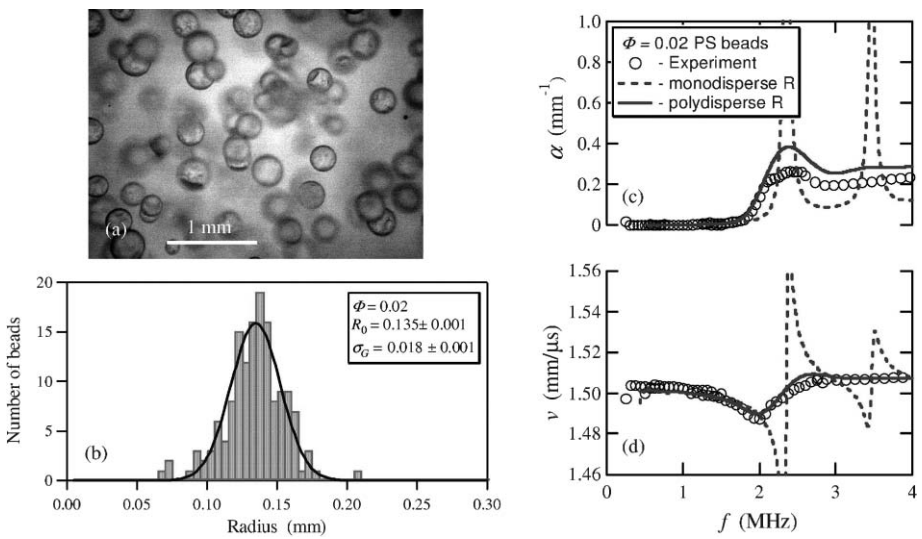

Fig. 2 (a) Sample image; (b) histogram of the particle size distribution; (c) and (d) frequency dependence of the attenuation and phase velocity for 2% PS beads in a 2% agar gel. In (b), the solid curve represents a Gaussian distribution that was fitted to the histogram, with R_0 and σ_G being the mean radius and standard deviation.

reliably used. For a medium in which the phase velocity varies with position, the scalar wave equation is

$$\left(\nabla^2 + \frac{\omega^2}{v^2(\vec{r})}\right)\Psi(\vec{r}) = 0\,, \tag{11}$$

where Ψ denotes the wave amplitude, and $v(\vec{r})$ is the local phase velocity at position r. This equation can be rewritten by adding and subtracting the term ω^2/v_0^2 as

$$\left[\nabla^2 + \frac{\omega^2}{v_0^2} - \varsigma(\vec{r})\right]\Psi(\omega,\vec{r}) = 0\,, \tag{12}$$

where $\varsigma(\vec{r}) = \omega^2/v_0^2 - \omega^2/v^2(\vec{r})$ represents the deviation from a uniform reference medium with phase velocity v_0. The Green's function for this problem is a solution of the wave equation [eqn (12)], with delta function excitation, $\delta(\vec{r}-\vec{r}')$, originating from a point source at $\vec{r}'$

$$\left[\nabla^2 + \frac{\omega^2}{v_0^2} - \varsigma(\vec{r})\right]G(\omega,\vec{r},\vec{r}') = \delta(\vec{r}-\vec{r}')\,. \tag{13}$$

In matrix notation, the Green's function, G, can be written in the form

$$\mathbf{G} = \mathbf{G}_0 + \mathbf{G}_0\mathbf{T}\mathbf{G}_0 \tag{14}$$

where $\mathbf{G}_0$ is the matrix representing the Green's function for a homogenous effective medium ($\varsigma = 0$), and $\mathbf{T}$ is the exact scattering operator, including all scattering events among the spheres, arising from the term $\varsigma(\vec{r})$ in eqn (12). By taking the ensemble average of eqn (14), we obtain $<\mathbf{G}> = \mathbf{G}_0 + \mathbf{G}_0<\mathbf{T}>\mathbf{G}_0$, so that all the effects of the scattering are taken into account by the ensemble-averaged scattering operator. The CPA condition for eqn (14) is $\langle\mathbf{T}\rangle = 0$, allowing the effective average velocity v_0 to be determined that is consistent with the criterion, $G = G_0$, that on average there should be no scattering in the effective medium if it is indeed an equivalent uniform medium. It is this CPA condition that cannot generally be satisfied in the intermediate frequency regime, requiring a different approach, such as the SpFA used here.

To find a solution using the SpFA in the intermediate frequency range, we further simplify eqn (14) by defining the self-energy operator, Σ_0, as

$$<\mathbf{G}>^{-1} = G_0^{-1} - \Sigma_0 \tag{15}$$

The self-energy operator represents all scattering effects calculated relative to a uniform medium where sound propagates with velocity v_0. In general, it is related to the scattering operator by $\Sigma = <\mathbf{T}>/(1 + <\mathbf{T}>\mathbf{G}_0)$. To leading order in the number N of the scattering particles per unit volume, $\Sigma_0 \approx N<\mathbf{t}_0> = Nf_0(\theta = 0)/4\pi$, where $<\mathbf{t}_0>$ is the average scattering operator for a single scatterer and $f_0(0)$ is the forward scattering amplitude (scattering angle $\theta = 0$). In the frequency and wave vector representation, the Green's function is then given by

$$\langle G(\omega,k)\rangle = \left(\frac{\omega^2}{v_0^2} - k^2 - \Sigma_0\right)^{-1}. \tag{16}$$

For the purposes of calculation, v_0 can be treated as a dummy variable and thus set to the value $v_0 = \omega/k$, so that the Green's function can be evaluated for any frequency and wavevector as

$$G(\omega, k) = -\Sigma_0^{-1}(\omega, k). \tag{17}$$

The spectral function, which gives the density of states as a function of frequency and wavevector, is then given by

$$S(\omega, k) = -\Im m(G) = \Im m[\Sigma_0^{-1}(\omega, k)]. \tag{18}$$

From eqn (18), it can be seen that the frequency and wavevector dependence of the spectral function can be used to identify the propagating modes of the system, since they correspond to modes with the least scattering having the smallest values of the self energy, and hence are given by peaks in the spectral function. Thus, by calculating the self-energy for each (ω, k) point and then determining the values of v_0 at the peaks of $S(\omega, k)$, the dispersion curve can be determined, and hence the effective medium velocity $v_{\text{eff}} = v_{0,\text{ peak}}$ at each frequency. Furthermore, the attenuation can be determined from the magnitude of the peaks of the spectral function *via* the optical theorem,[30] or directly by averaging the square of the scattering amplitude over all angles, $\alpha = 4\pi N\int_0^\pi |f_0(\theta)|^2 \mathrm{d}\theta$. These calculations require knowledge of the longitudinal and shear velocities in the PS beads and the longitudinal velocity in the matrix, as well as the densities of both media and the volume fraction of PS beads. The model was also extended to account for intrinsic attenuation in the PS beads; however, this attenuation is sufficiently small that it had only a very small effect on the predicted properties over the frequency range studied, and thus was not a critical parameter in these calculations. The parameters used in the calculations for this PS gel system are listed in Table 1, and were mostly known for our sample from independent measurements.

Fig. 2c and d show a comparison of the velocity and attenuation calculated using the SpFA with our experimental results. These calculations were performed both for monodisperse beads with R_0 equal to the average value (dashed curves), and for a Gaussian size distribution obtained from the image analysis (solid curves). Good agreement between theory and experiment was obtained in the second case, especially for the velocity. For the attenuation, the predicted magnitude is somewhat larger, although the shape of the peak, including its width, is still accurately predicted. Based on this good agreement, it is reasonable to infer that the bead size distribution can itself be determined from ultrasonic measurements using this approach.

c) Gel systems containing PS beads and bubbles

Having established the ultrasonic methods that can be used to determine the size distribution of both bubbles and solid particles when dispersed separately in a gel, we next examined the applicability of the methods to a system containing *both* bubbles and PS beads. The sample prepared for this purpose is shown in Fig. 3a and b, where a typical image and a histogram of the inclusion sizes are presented. One can see that the size distribution is much broader than for both previous cases, and that it is almost impossible to discriminate between bubbles and beads by image analysis of the picture.

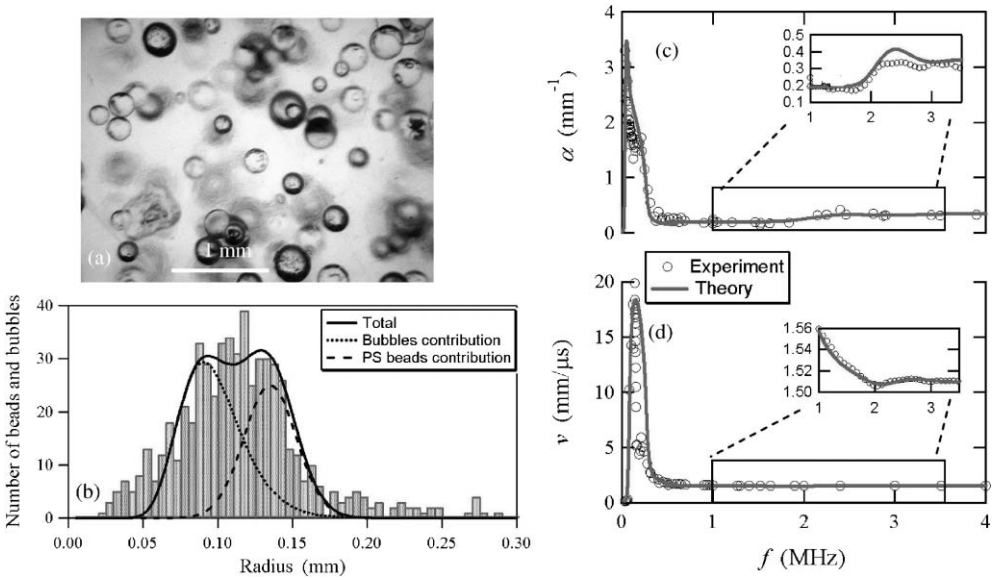

Fig. 3 Data for a sample containing both 1% PS beads and 0.5% bubbles in agar gel: (a) sample image, (b) histogram of the size distribution measured by image analysis (vertical bars) and by ultrasonic spectroscopy (curves), (c) and (d) frequency dependence of the ultrasonic attenuation and phase velocity.

By contrast, both the attenuation and phase velocity show clear evidence of two distinct resonance peaks located at different frequencies (see Fig. 3c and d). Thus, the two types of scatterer can be clearly resolved in the ultrasonic data even though their sizes are comparable. To display the high frequency peak due to the PS beads more visibly, the figures also contain inserts of the high-frequency region with a magnified vertical scale, since the changes in phase velocity and attenuation are much smaller for PS beads than for bubbles when their concentrations are similar. Note that, even though the velocity insert shows a decreasing background with frequency due to the shoulder of the bubble resonance, the PS resonance is still clearly resolvable for velocity as well as for attenuation.

To demonstrate that the ultrasonic data can be used to determine the concentration and size distribution of the inclusions, theoretical calculations were performed separately in the low and high frequency regions using the known acoustic properties of the three constituents. The solid curves in Fig. 3c and 3d are the best fit of the theories to the experimental data, with the size distributions and concentrations of the bubbles and beads as the unknown parameters. Very good overall agreement is shown between these theoretical predictions and the experimental data in both frequency ranges. It was found from these fits that the parameters of the distributions for the PS beads are $\Phi = 0.01$, $R_0 = 0.135 \pm 0.005$ mm, and $\sigma_G = 0.018 \pm 0.005$, while for the bubbles $\Phi = 0.005$, $R_0 = 0.10 \pm 0.01$ mm, and $\sigma_{LN} = 0.22 \pm 0.02$, respectively. The curves in Fig. 3b are the size distributions for both PS beads and bubbles obtained from the ultrasonic experiments, as well as the combined distribution. These results are compared with the histogram obtained using image analysis, shown as the vertical bars. The correspondence is remarkably good. Our ultrasonic determinations are superior to image analysis in that the bubbles can be distinguished from the solid inclusions, enabling the concentrations and size distribution parameters to be determined. Another strength of the acoustic method is the possibility of applying the technique to opaque media, where optical evaluation of even the total distribution of inclusions is impossible.

Conclusions

Ultrasonic spectroscopy has been used to demonstrate that bubbles have a huge effect on the acoustic properties of a model aerated food system. A broad peak in the attenuation as a function of frequency was shown to arise due to resonance effects, and is accompanied by a pronounced variation in the ultrasonic velocity. This behaviour of the velocity and attenuation was well described by a model for the resonant interactions of ultrasonic waves with bubbles in a soft material. The associated bubble-size-dependent resonance frequency occurred when the ultrasonic wavelength was much larger than the size of the bubbles. The scattering of ultrasound from solid inclusions (polystyrene beads) of similar size to the bubbles was observed at much higher frequencies and was successfully modelled with an effective medium model based on a spectral function approach. Thus, both experiment and theory demonstrated that the ultrasonic signatures of bubbles and solid inclusions can be distinguished, even when the inclusions are of comparable sizes.

In this paper, we have exploited the acoustic resonances of the inclusions to demonstrate the feasibility of directly monitoring their size distributions. While the current experiments have been performed on samples with relatively low concentrations (up to 2%) and large sizes ($\sim$100 μm) of inclusions, there is nothing in principle that should preclude extending the approach to the much higher concentrations or smaller particle sizes often found in soft materials. At high

concentrations, for example, our SpFA model has been applied successfully to interpret experimental data on suspensions of glass beads at volume fractions up to 63%, where this effective medium approach provides remarkably accurate results.[23,35,36] While high attenuation can limit the range of concentrations and sizes of inclusions that can be investigated in transmission experiments, reflection techniques based on acoustic impedance differences do not suffer from this limitation; they should allow inclusion sizes to be studied down to the low micron range by tuning the ultrasonic frequency to match the resonance condition.

The resonance spectroscopy methods demonstrated in this paper complement the well established particle sizing approach based on the work of Epstein and Carhart[37] and Allegra and Hawley;[38] their theoretical models for the frequency dependence of the ultrasonic attenuation in the long wavelength regime ($\lambda \gg R_0$) have been extensively used as the basis for measuring the particle size distribution and concentration in colloids and dispersed systems. Because of the sharp spectral features of resonances, our approach may be especially useful for precise particle and bubble sizing in heterogeneous materials such as foods, where the sizes of the inclusions are often large enough to be easily accessible by resonance spectroscopy.

Our results on this model system may be viewed as an important step towards the use of ultrasonic resonance techniques to characterize real functional foods containing bubbles and solid nutrient inclusions. Because both solid and gas inclusions can be detected simultaneously, even when they have comparable sizes, ultrasound has considerable potential as a non-invasive technique for evaluating quality impairment arising from bubble-nutrient interactions during the manufacture of high quality functional foods. This will enable nutritional benefits to be maximized while maintaining good control over food microstructures, thereby helping to ensure consumer acceptability.

Acknowledgements

Support of this research by NSERC, the AFMNet Network Centre of Excellence and Manitoba Centres of Excellence Foundation is gratefully acknowledged.

References

1 A. Donald, *Nat. Mater.*, 2004, **3**, 579–581.
2 R. Mezzenga, P. Schurtenberger, A. Burbidge and M. Michel, *Nat. Mater.*, 2005, **4**, 729–740.
3 T. S. Awad, M. A. Rogers and A. G. Marangoni, *J. Phys. Chem. B*, 2004, **108**, 171–179.
4 Y. W. Chen and M. R. Mackley, *Soft Matter*, 2006, **2**, 304–309.
5 N. Garti, A. Spernath, A. Aserin and R. Lutz, *Soft Matter*, 2005, **1**, 206–218.
6 M.J. Brown, M. G. Ferruzzi, M. L. Nguyen, D. A. Cooper, A. L. Eldridge, S. J. Schwartz and W. S. White, *Am. J. Clin. Nutr.*, 2004, **80**, 396–403.
7 C. M. Hasler, *J. Am. Coll. Nutr.*, 2000, **19**, 499S–506S.
8 Anon., *J. Am. Diet. Assoc.*, 2004, **104**, 814–826.
9 C. H. Halsted, *Am. J. Clinical Nutr.*, 2003, **77**, 1001S–1007S.
10 Z. Gan, P. R. Ellis and J. D. Schofield, *J. Cereal Sci.*, 1995, **21**, 215–230.
11 S. Lee, S. Kim and G. E. Inglett, *Cereal Chem.*, 2005, **82**, 120–124.
12 M. D. Eisner, H. Wildmoser and E. J. Windhab, *Colloids Surf., A*, 2005, **263**, 390–399.
13 E. Dickinson, *Colloids Surf., B*, 2001, **20**, 197–210.
14 A. D. Gopal and D. J. Durian, *J. Colloid Interface Sci.*, 1999, **213**, 169–178.
15 D. Weaire and S. Hutzler, *The Physics of Foams*, Oxford University Press, Oxford, 1999.
16 H. A. Makse, J. Brujić and S. F. Edwards, in *The Physics of Granular Media*, ed. H. Hinrichsen and D. E. Wolf, Wiley-VCH, 2004, pp. 1–51.
17 G. Debrégeas, P.-G. de Gennes and F. Brochard-Wyart, *Science*, 1998, **279**, 1701–1704.
18 A. D. Gopal and D. J. Durian, *Phys. Rev. Lett.*, 2003, **91**, 188303.
19 P. Babin, G. Della Valle, R. Dendievel, N. Lassoued and L. Salvo, *J. Mater. Sci.*, 2005, **40**, 5867–5873.
20 M. J. W. Povey, *Ultrasonic Techniques for Fluids Characterization*, Academic Press, San Diego, 1997.
21 H. Kuttruff, *Ultrasonics: Fundamentals and Applications*, Elsevier Applied Science, London, 1991.
22 *Acoustic Resonance Scattering*, ed. by H. Überall, Gordon and Breach, Philadelphia, 1992.
23 M. L. Cowan, K. Beaty, J. H. Page, Zhengyou Liu and Ping Sheng, *Phys. Rev. E*, 1998, **58**, 6626–6636.
24 V. Leroy, Y. Fan, A. L. Strybulevych, G. G. Bellido, J. H. Page and M. G. Scanlon, in *Bubbles in Food 2: Novelty, Health & Luxury*, ed. G. M. Campbell, M. G. Scanlon and D. L. Pyle, AACC Press, 2007, in press.
25 K. W. Commander and A. Prosperetti, *J. Acoust. Soc. Am.*, 1989, **85**, 732–746.
26 T. G. Leighton, *The Acoustic Bubble*, Academic Press, San Diego, 1994.
27 V. N. Alekseev and S. A. Rybak, *Acoust. Phys.*, 1999, **45**, 535–540.
28 U. Hamhaber, F. A. Grieshaber, J. H. Nagel and U. Klose, *Magn. Reson. Med.*, 2003, **49**, 71–77.
29 A. B. Wood, *A Textbook of Sound*, Bell, London, 1941.
30 Ping Sheng, *Introduction to Wave Scattering, Localization, and Mesoscopic Phenomena*, Academic Press, San Diego, 1995.
31 X. D. Jing, P. Sheng and M. Y. Zhou, *Phys. Rev. Lett.*, 1991, **66**, 1240–1243.
32 X. D. Jing, P. Sheng and M. Y. Zhou, *Phys. Rev. A*, 1992, **46**, 6513–6534.
33 *American Institute of Physics Handbook, 3rd edn*, ed. D. E. Gray, McGraw-Hill, New York, 1972.
34 L. O. Adjadj, G. Storti and M. Morbidelli, *Langmuir*, 2003, **19**, 3953–57.
35 J. H. Page, Ping Sheng, H. P. Schriemer, I. Jones, Xiaodun Jing and D. A. Weitz, *Science*, 1996, **271**, 634–637.
36 H. P. Schriemer, M. L. Cowan, J. H. Page, Ping Sheng, Zhengyou Liu and D. A. Weitz, *Phys. Rev. Lett.*, 1997, **79**, 3166–3169.
37 P. S. Epstein and R. R. Carhart, *J. Acoust. Soc. Am.*, 1953, **25**, 553–565.
38 J. R. Allegra and S. A. Hawley, *J. Acoust. Soc. Am.*, 1972, **51**, 1545–1564.

